Space Object Temperature Determination from Multi-Band Infrared Measurements

Charles Paxson, Hilary E. Snell, and James M. Griffin
Atmospheric and Environmental Research, Inc.

Kathleen Kraemer, Steve Price, and Mike Kendra
Air Force Research Laboratory, Space Vehicles Directorate

Don Mizuno
Boston College

1. Abstract

We describe a technique to determine the temperature of a Resident Space Object (RSO) from multiple infrared (IR) bands. The characteristic temperature of an object is the temperature of the Planck function that has the closest least squares fit to the observed irradiance in at least three infrared bands. The characteristic temperature and the effective solid angle are free parameters in a formulation that requires simultaneous minimization, across all bands, of chi-square expressions using modeled irradiances and the measured irradiances and their errors. Solutions are determined from a multi-dimensional Levenberg-Marquardt fitting algorithm. The advantage of this approach is that it provides a single, best-fit solution to the RSO modeled as a gray body radiator. In contrast, a 2-band (color) temperature approach using three or more bands produces different solutions for different band combinations with no objective way of determining which solution is best.

We apply this technique to IR measurements of RSOs obtained by the Midcourse Space Experiment (MSX) satellite. The AFRL MSX database of serendipitous RSO observations contains multi-band IR measurements for hundreds of objects, including payloads, rocket bodies, and debris. Using this technique, we have obtained object characteristic temperatures and Infrared Cross Sections (IRCS) under a large variety of phase angle and solar illumination conditions, including eclipse. We examine specific cases in detail. We also compare and contrast results for population groups based on orbit type (LEO – low earth orbit, MEO – medium earth orbit, and GEO – geostationary earth orbit) and other parameters of interest. In addition, we look at a number of cases where color and characteristic temperatures and solid angles have been determined for the same object measurements and show that the characteristic parameters are more consistent with the Planck function model when expressed as their equivalent isophotal emissions.

2. Introduction

Understanding the intended function and current state of an RSO can be difficult due to observational considerations, including the size of the object, whether or not it is spinning, and the atmospheric and geometric conditions under which the object is observed. In addition to radar and optical observations, infrared measurements allow for the calculation of the RSO temperature and may provide clues to the composition and operational status of an object. Because an RSO may be warm by internal heating, intercepted radiation from the Sun and Earth, recent reaction jet burns, friction from atmospheric drag, etc., analysis of the time rate of change in temperature as the various thermal inputs change may be used to type the object. Using RSOs measured by the Spatial Infrared Imaging Telescope (SPIRIT III) aboard the MSX satellite [1] we have developed a process to determine the RSO temperature. From this work we have produced a catalog which includes the apparent temperature of objects within our MSX database of serendipitous RSO observations [2]. In this paper we describe the methods used to calculate these RSO temperatures from the SPIRIT III radiometry and present results and evaluations of our method.

2.1. Characteristic, Color, and Brightness Temperatures

For this study we have collected a set of serendipitous RSO observations and determined the apparent temperature of the objects using data from the SPIRIT III radiometer. Each RSO may be modeled as a gray body radiator with in-band irradiance from an object defined as:

$$I = \Omega \int_0^\infty \varepsilon(\lambda) RSR(\lambda) B(\lambda, T) d\lambda = \Omega_{\varepsilon A} \int_0^\infty RSR(\lambda) B(\lambda, T) d\lambda \qquad (1)$$

where Ω is the solid angle, $\varepsilon(\lambda)$ is the spectral emissivity as a function of wavelength λ, RSR(λ) is the relative spectral response of the sensor, and B(λ, T) is the blackbody Planck function (W cm^{-2} μm^{-1} sr^{-1}) at temperature T (K). Here, the emissivity is assumed to be independent of wavelength and the effective solid angle $\varepsilon\Omega = \Omega_{\varepsilon A}$ (or Ω_{eff}) is outside of the integral to indicate that the emissive area is considered to be a constant.

Information about the four SPIRIT III bands used in this study is shown in Table 1. Note that we did not consider Band B as it is dominated by reflected sunlight rather thermal emission.

Table 1: Integration Limits for the In-band Radiance Calculations.

Sensor Band	Minimum Wavelength (μm)	Maximum Wavelength (μm)	Isophotal Wavelength (μm)
A	5.88	11.19	8.28
C	10.53	13.70	12.13
D	12.66	16.65	14.65
E	16.95	28.50	21.34

The most robust way to determine the temperature of the object is to use data from all four bands. However, in some cases only a subset of this data is available for a particular RSO observation, due to channel saturation, noise or other effects. Thus we have implemented three methods for deriving the temperature, depending on the number of bands in which an RSO was detected with sufficient signal strength. In order of decreasing robustness, these are: the "characteristic" temperature, for RSOs with detections in 3 or 4 bands; the "color" temperature, for those with detections in only 2 bands; and the "brightness" temperature, for those with detections only in a single band. This is shown schematically in Figure 1.

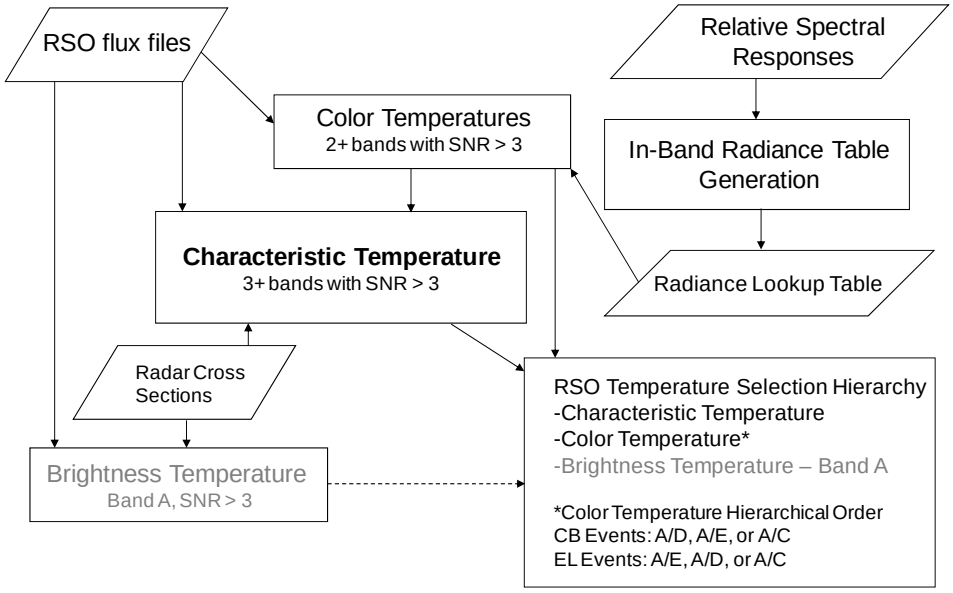

Figure 1: Measured fluxes from RSO candidates are used to derive the object temperature. For each RSO, the color temperature and the radar cross section are used as initial estimates ("seed values") for the characteristic temperature determination algorithm. The final output to the catalog depends upon the number of bands for which data is available.

The brightness temperature is the temperature of an ideal blackbody whose radiant energy in a single wavelength band is the same as that of the observed source. It is calculated from the inverse of the Planck function given a

single radiance value. The size of the source, distance from the observer and the emissivity must be known (e.g., the radar cross section (RCS) for the size), or assumed to estimate the brightness temperature. Because of the uncertainty in the *a priori* knowledge of the cross sectional areas, the brightness temperature will not be discussed further. Color temperature is derived from the ratio of irradiances in two different spectral bands and, therefore, eliminates common factors such as the emissivity and solid angle. In contrast, the characteristic temperature is derived by fitting a single Planck function to multi-band irradiances to simultaneously determine the blackbody temperature and effective solid angle representative of the measurements. The color and characteristic temperatures are discussed in more detail in the following sections.

2.1.1. Color Temperature

The RSO color temperature T_{color} is defined as the temperature of an object that will produce an in-band irradiance ratio equal to that of two measured in-band radiances. Because the RSO geometric parameters (solid angle and cross-sectional area) are the same for all bands at the time of observation, their radiance ratios and irradiance ratios are identical. Six color temperatures may be derived from the four SPIRIT III band A, C, D, and E irradiance measurements, where the observed band ratios are linearly interpolated to obtain the color temperature that corresponds to the measured ratio. Once a color temperature has been derived, a measured irradiance may used to determine the effective solid angle $\Omega_{\varepsilon A}$ of the RSO by rearranging Equation (1):

$$\Omega_{\varepsilon A} = I / \int_0^\infty RSR(\lambda) B(\lambda, T_{color}) d\lambda \qquad (2)$$

2.1.2. Characteristic Temperature and Solid Angle

The characteristic temperature is the most robust method for determining RSO temperature. It is derived by simultaneously fitting the in-band measured irradiances from at least three SPIRIT III bands to the irradiances I_{Band}(model) derived from Equation (1). The characteristic temperature, T_{char}, and the effective solid angle, $\Omega_{\varepsilon A}$, are free parameters whose solution is obtained by minimizing the χ^2 in the formulation:

$$\chi^2 = \sum [(I_{Band}(\text{measured}) - I_{Band}(\text{model}))/\sigma_{Band}]^2 \qquad (3)$$

where I_{Band}(measured) is the measured in-band irradiance, σ_{Band} is the estimated irradiance uncertainty, and the summation is over the available bands.

The minimum χ^2 is determined from the simultaneous numerical solution of $\partial\chi^2 / \partial\Omega_{\varepsilon A} = 0$ and $\partial\chi^2 / \partial T = 0$. The RSO characteristic temperature is computed if SPIRIT III obtained irradiance measurements in 3 or 4 bands with SNR>3. Thus, the characteristic temperature is the temperature of the Planck function that has the closest least-squares fit to the observed irradiance in at least 3 of the SPIRIT III long-wave infrared bands.

The free parameters, $\Omega_{\varepsilon A}$ and T, are determined from the standard multi-dimensional Levenberg-Marquardt (LM) nonlinear least-squares fitting algorithm [3]. The LM algorithm requires initial estimates of $\Omega_{\varepsilon A}$ and T. The initial temperature estimate is the color temperature with the smallest relative uncertainty while the initial effective solid angle is estimated from the RCS and the range from the RSO and MSX ephemerides: Ω_0= RCS/range^2. The effective infrared (IR) cross-sectional area IRCS may be computed from the effective solid angle by means of IRCS=$\varepsilon A=\Omega_{\varepsilon A}$x range^2.

In addition to the standard χ^2 minimization, the "quality of fit" parameter Q is computed for each RSO:

$$Q(\chi^2; n) = \frac{1}{\Gamma(n)} \int_{\chi^2}^{\infty} P(\chi'^2; n) d\chi'^2 \qquad (4)$$

where n is the degrees of freedom in the fit (1 for 3 bands, 2 for 4 bands), Γ is the gamma function, and P is probability distribution of χ^2 [3],[4],[5]. The fit is believable for Q > 10%, and hence the data are well-described by the model in Equation 1. For 0.1% < Q < 10%, the model may still be viable if the uncertainties are non-normal or underestimated.

3. Results and Evaluation

3.1. Characteristic and Color Temperature Results

Good agreement was found in general between the color and characteristic temperatures of an RSO. Figure 2 compares the characteristic temperature to the highest precision color temperature (i.e. smallest $\sigma_{Tcolor}/T_{color}$); this was the color temperature used to seed the characteristic fit.

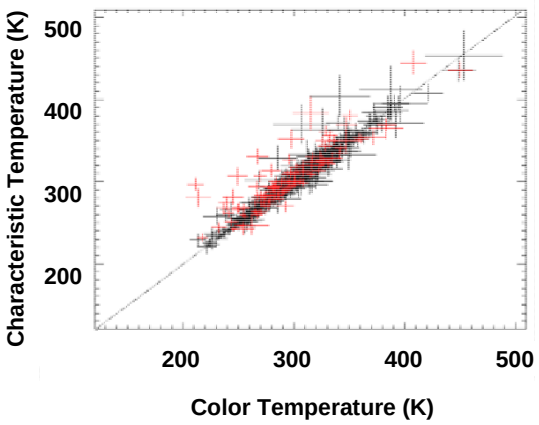

Figure 2: T_{color} vs. T_{char} with 1σ error bars. Characteristic temperatures with Q > 0.1 are shown in black and those with Q < 0.1 in red. While multiple color temperatures may be formed from the 3 and 4-band data, only the initial seed temperature, i.e. the highest precision color temperature, is shown.

The results of the characteristic temperature fits for a representative sample of cases are shown in Figure 3 through Figure 6; these results are also summarized in Table 2. These results are arranged according to the number of bands used for characteristic temperature and the quality of fit parameter, Q. Figure 3 shows results for RSOs with observations in 4 bands and Q > 0.1, Figure 4 shows 4-band results for Q < 0.1, Figure 5 shows 3-band results for Q > 0.1, and Figure 6 shows 3-band results for Q < 0.1. The measurements are plotted with an "x" together with the associated 1σ uncertainties. The solid curve shows the Planck function for the derived characteristic temperature while the dotted curve shows the Planck function corresponding to the derived color temperature.

Table 2: Sample Fit Results

		Characteristic				Color		
RSO	Figure	Band	T (K)	Ω (sr)	Q (%)	Band	T (K)	Ω (sr)
1	3	4	298.2	1.0E-13	12.1	A/E	301.3	9.8E-14
2	5	3	292.1	4.5E-15	64.5	A/D	297.1	4.1E-15
3	3	4	301.5	4.2E-15	12.2	A/E	268.3	8.3E-15
4	5	3	295.8	7.6E-14	1.9	A/E	288.5	7.9E-14
5	4	4	354.8	4.3E-15	<0.1	A/D	354.4	4.4E-15
6	6	3	383.0	1.8E-15	<0.1	A/E	314.9	4.7E-15
7	4	4	321.4	1.9E-13	<0.1	A/E	329.1	1.5E-13
8	6	3	288.7	8.9E-14	<0.1	A/E	277.4	9.3E-14

In general there is good agreement between measured and computed values. Figure 5 and Figure 6 demonstrate that three band characteristic temperature determination process works well, while Figure 4 and Figure 6 show that low Q values do not necessarily indicate a poor temperature determination. One possible explanation is that the uncertainty estimates obtained from measurements are too small, resulting in low Q values but good temperature

fits. We note the robustness of the characteristic temperature method through inspection of RSO 3. For this measurement our process found that the A/E color ratio was the most precise combination for the color temperature. However, the resulting color temperature is biased as Band E is an outlier with a relatively small uncertainty. In contrast, the characteristic temperature fit conforms to 3 of the 4 band irradiances. This case demonstrates that the characteristic temperature method is robust against outliers because it utilizes the uncertainty and the bias for the irradiance of each band, as may be seen by the relatively good fit for RSO 3 with a reasonably high Q value of 12.2%.

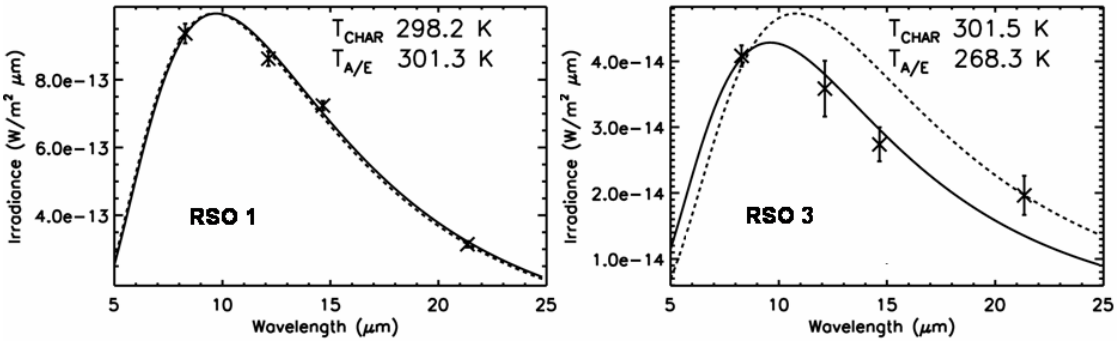

Figure 3: Characteristic Fits to Data. Four bands fit, Q > 0.1.

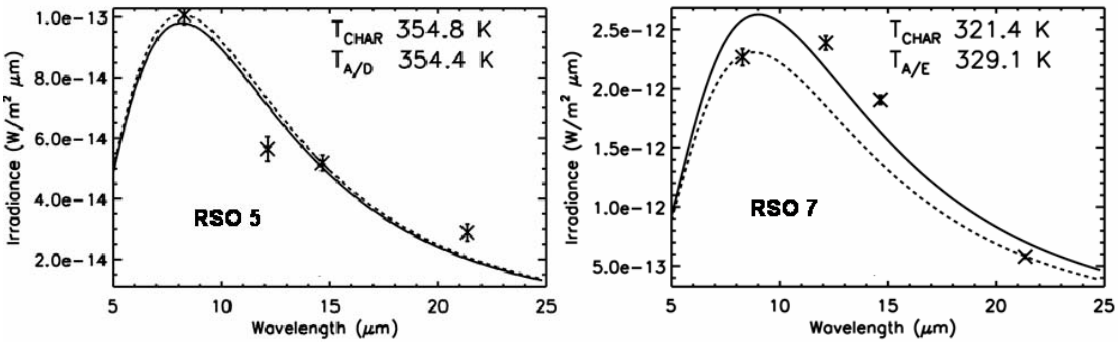

Figure 4: Characteristic Fits to Data. Four bands fit, Q < 0.1.

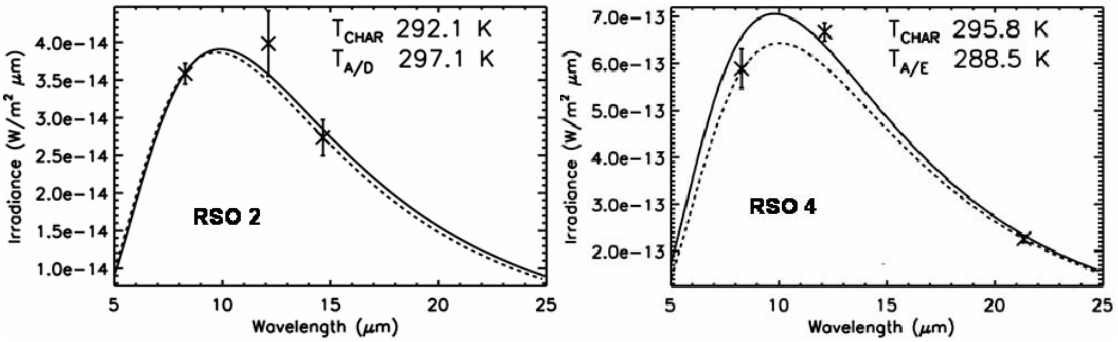

Figure 5: Characteristic Fits to Data. Three bands fit, Q > 0.1.

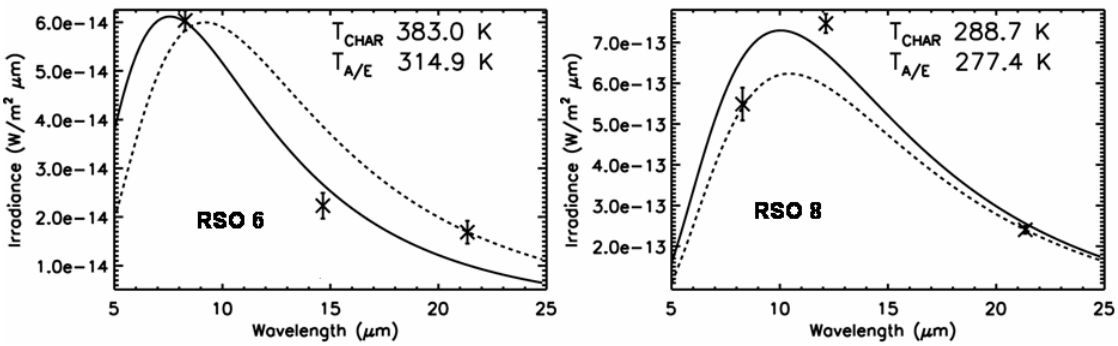

Figure 6: Characteristic Fits to Data. Three bands fit, Q < 0.1.

3.2. Comparison of Characteristic and Radar Solid Angles

The derivation of the characteristic temperature simultaneously solves for the temperature and the effective solid angle $\Omega_{\varepsilon A}$. Figure 7 presents a comparison between $\Omega_{\varepsilon A}$ and the solid angles computed from radar cross section and range. The RSOs are separated into those with ranges less than 15,000 km and those greater than 15,000 km. For nearby objects the results show good agreement for objects with solid angles down to about 10^{-14} sr. In contrast, the RSOs with ranges greater than 15,000 km show poor agreement between $\Omega_{\varepsilon A}$ and the radar-derived solid angle. The lack of objects with $\Omega_{\varepsilon A}<10^{-15}$ sr implies that this corresponds to the detection limit of SPIRIT III which is consistent with the known detector characteristics. Similarly, the IR-derived cross sectional areas are well-correlated with the radar cross sections for ranges less than 15,000 km but not above 15,000 km (shown in the lower panels of Figure 7). The points circled in the lower right panel have identical RCS values. Most of the objects are payloads with IR cross sections of ~4-28 m^2. The RCS values for those RSOs are from the same radar site so this likely reflects a default value for the radar site, although we have been unable to confirm that. We conclude that although the radar cross section data are useful for IR analysis of LEO objects, they are of limited value for IR applications to high earth orbit (HEO) and GEO objects. The cross-sectional areas obtained from the infrared thermal analysis are reliable parameters for describing the true physical size of objects at all distances.

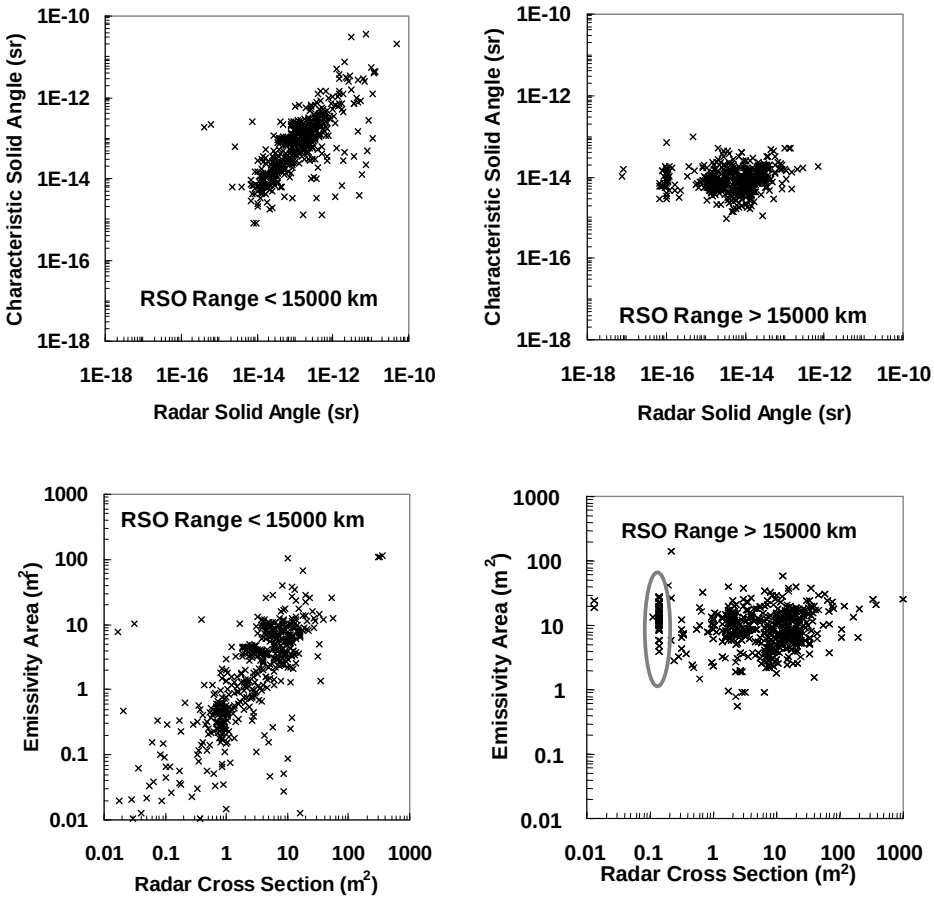

Figure 7: Comparison of the IR- vs. radar-derived solid angles and areas. (Top left) Ω_{radar} vs. $\Omega_{\varepsilon A}$ for RSOs with ranges < 15,000 km. (Top right) Ω_{radar} vs. $\Omega_{\varepsilon A}$ for RSOs with ranges > 15,000 km. (Bottom left) RCS vs. IRCS (emissivity area) for RSOs with ranges < 15,000 km. (Bottom right) RCS vs. IRCS for RSOs with ranges > 15,000 km. The circled objects all have identical RCS values although the IR-derived areas vary by more than an order of magnitude.

4. Preliminary Analyses of Temperature Trends

4.1. Temperature and Solar Illumination

The thermal balance of an RSO is primarily determined by the rate at which photons are absorbed and emitted. Other forms of heat exchange depend upon frequent collisions with atomic or molecular gases, such as drag interaction with the atmosphere, or heating from internal power sources. The lowest altitude at which an RSO was observed was 300 km, well above most of the atmosphere, and internal heat sources are minor contributors when the RSO is sunlit. A detailed description of the energy balance may be possible for objects of known size, shape, orientation, materials, material properties, and thermal history. However, our knowledge of these parameters is limited and exquisite modeling is not possible for most objects. The primary advantage of the current RSO database is that the data herein provide many of the answers for large portions of the RSO population.

For example, Figure 9 shows the RSO characteristic temperature as a function of the solar illumination parameter, which is a measure of the number of solar diameters the Sun is above or below the horizon with respect to the RSO at the time of observation. Values less than zero indicate that the object was in eclipse while values greater than one indicate the object was fully sunlit. Since the thermal balance for objects in the Earth's shadow is very different from that when the object is illuminated (and therefore heated), an abrupt transition to higher (or lower) temperature should occur when an object passes through the transition region. The data in Figure 8 confirm this, showing a

noticeable transition from an average eclipsed RSO temperature of 280 K to an average of 320 K for objects near the terminator, defined as the illumination range within 20 solar diameters. Also contributing to the temperature transition region in the plot are the RSOs that will be entering eclipse shortly so they are near their maximum temperature.

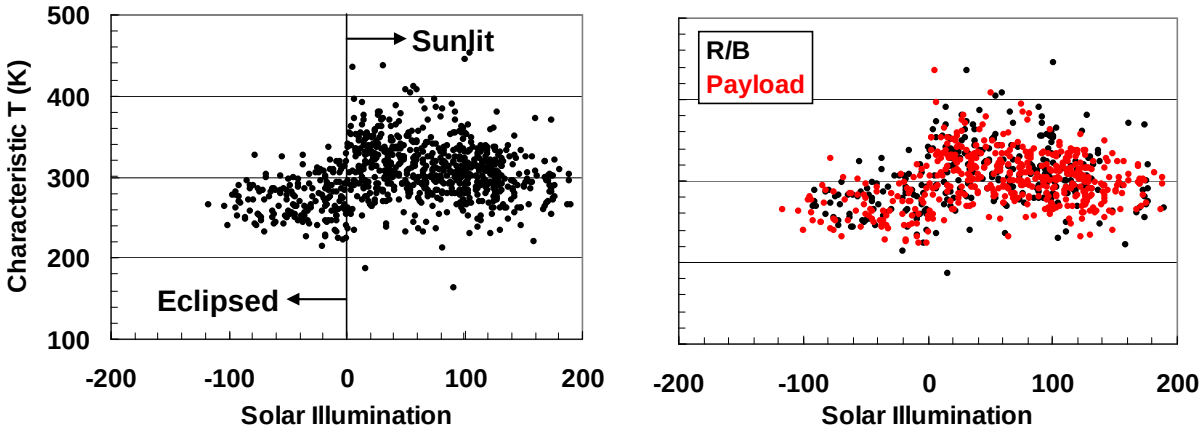

Figure 8: Solar Illumination parameter vs. characteristic temperature (left) for the whole population and (right) for the payloads (red) and R/Bs (black). Negative solar illumination indicates eclipse conditions whereas positive values mean the RSO was sunlit.

Since each object in the catalog is identified, the temperature characteristics with respect to RSO type may be examined. The right-hand panel in Figure 8 plots the temperature and illumination values for the payloads in red and for the rocket bodies (or boosters, R/Bs) in black. The payloads and R/Bs have similar thermal characteristics with respect to the solar illumination parameter. This suggests that although material properties may be important for object identification and characterization, the measured temperatures do not provide good discrimination between these two broad populations. To first order, the thermal signatures are more dependent on solar illumination and illumination history than on object type. It also supports our supposition that internal heat sources, which payloads might have but R/Bs would not, play at most a minor role in the heat balance in the general RSO population.

4.2. Observation of the Hubble Space Telescope

As discussed above, observations in two bands permit a color temperature to be derived; the IR emissive area is calculated from the blackbody equation using the color temperature solution. Schulenburg et al. [6] noted some interesting trends obtained during the tracking of GPS satellites. For that analysis each scan was treated as an independent observation, and a plot of emissive area (εA) versus temperature appeared to provide information that could be useful in object characterization.

Figure 9 (left panel) shows an example for a similar event, in particular an observation of the Hubble Space Telescope (HST). One would expect the color temperature and the emissive areas to show ordered variations with respect to time. The left hand panel of Figure 9 shows the derived emissive area as a function of color temperature while the right hand panel displays the time series of these parameters. Because the HST observation is not centered in the mirror scan field of regard but is offset, resulting in non-uniform time steps, the data are plotted versus measurement number for clarity. On average, the measurement points are about three seconds apart and the color temperatures alternate between high and low for portions of the measurement series. This alternation may be related to the sawtooth pattern noted by Price et al. which they speculate is due to the systematic bias in calibrating the relative responses between the individual detector columns [7],[8]. This bias was estimated and included in the uncertainty used in the temperature determination. Even though the measurements were made in succession, the color temperature error can produce a bias in the true εA that is anti-correlated with the formal changes in temperature. For example, in the particular sequence of three measurements highlighted on the right side of Figure

9 we see that these correspond to extreme cases in the left panel this figure. A formal propagation of errors for both the color temperature and εA is necessary to properly interpret the derived quantities.

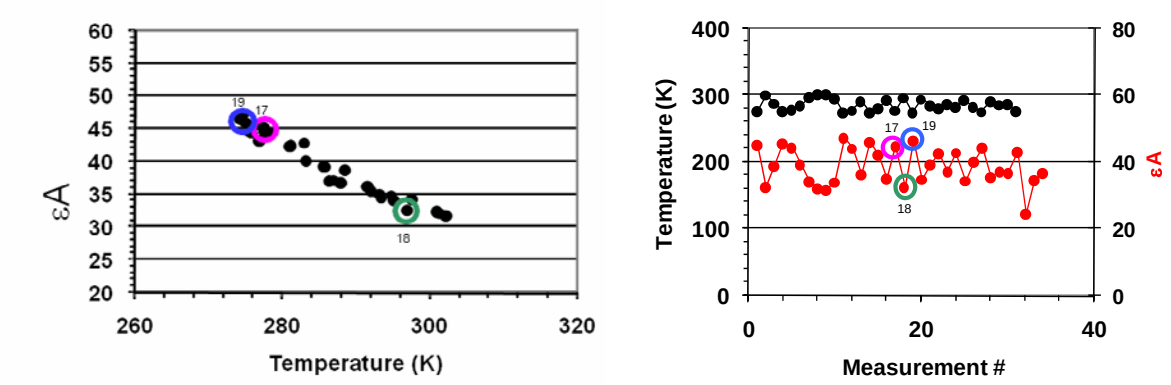

Figure 9: (left) εA versus T_{color}(A/D) for an EM12 observation of the Hubble Space Telescope. (right) Temporal evolution of T_{color} (upper curve, black points, left hand axis) and εA (lower curve, red points, right hand axis). Measurements were slightly irregular but average ~3 seconds apart.

5. Conclusions

The goal of this poster is to inform the Space Situational Awareness community of a robust technique to determine a space object's temperature and emissive cross sectional area from multi-band infrared measurements. We outlined the method and described results. In order to estimate the characteristic T and IR $\Omega_{\varepsilon A}$ we modeled space objects as gray radiating bodies with emissivities independent of wavelength. To derive the initial estimates, T_{color} and Ω_{radar}, that seed the nonlinear least squares Levenberg-Marquardt algorithm, we utilized MSX pointing information, radar estimates of space objects' cross-sectional areas, the known ephemerides of the objects, and our highest precision color temperature. We showed that the highest precision color temperature agreed with the characteristic generally, but a slight skew in the relationship was noted. We showed that the IR $\Omega_{\varepsilon A}$ agrees with Ω_{radar} for RSOs observed within a range of 15,000 km, but beyond the 15,000 km range the IR $\Omega_{\varepsilon A}$ and Ω_{radar} do not agree. Our interpretation is that the radar values for ranges greater than 15,000 km may not be reliable. We showed that the characteristic temperature is robust, appropriately weighting in-band irradiance and its associated uncertainty, whereas a color temperature may be significantly biased owing to a low quality irradiance measurement. The results from the population analyzed produced consistent results, for example the sunlit space objects were generally warmer, space objects cooled as they entered eclipse, and the radiant intensity was greater for larger sized and hotter objects. We also found that the time series variations in color temperature and εA were anti-correlated, leading to a relationship in εA versus temperature plots that may be due to the propagation of measurement errors in the sequential, color-based methodology rather than physically real variations in the object characteristics.

6. References

[1] Mill, J. D., R. R. O'Neil, S. Price, G. J. Romick, O. M. Uy, E. M. Gaposchkin, G. C. Light, W.W. Moore Jr., T. L. Murdock, & A.T. Stair Jr. (1994), Midcourse Space Experiment: Introduction to the Spacecraft, Instruments and Scientific Objectives, *J. Spacecraft and Rockets*, **31**, 900 – 907.

[2] Kraemer, K. E., Price, S. D., Kendra, M. J., Mizuno, D. M., Paxson, C., Griffin, J., Kuchar, T. A., and Cowley, J. E. *A Catalog of Resident Space Object Observations by the Midcourse Space Experiment*, AFRL Technical Report AFRL-RV-TR-2008-1009, 2008.

[3] Press, W. H., S. A. Teukolsky, W. T. Vettering, & B. P. Flannery (1992), *Numerical Recipes in C* (2nd Edition; Cambridge: Cambridge University Press).

[4] Barlow, R. J. (1989), *Statistics: A Guide to the Use of Statistical Methods on the Physical Sciences*, Chichester: John Wiley & Sons, Ltd.

[5] Bevington, P. R. (1969), *Data Reduction and Error Analysis for the Physical Sciences* (New York: McGraw-Hill, Inc.).

[6] Schulenburg, N. W., B. Klem, J. M. Lyons, N. Caraballo, & G. C. Light (1998), *Analysis of Observations from the MSX RSO Experiment*, DTIC ADD 950 617.
[7] Price, S. D., C. Paxson, C. Engelke, & T. L. Murdock (2004a), Spectral Irradiance Calibration in the Infrared XV. Calibration of Standard Stars by the Midcourse Space Experiment, *Astron. J*., **128**, 889 – 910.
[8] Price, S. D., C. Paxton, C. Engelke, T. L. Murdock, & K. E. Kraemer (2004b), *Absolute Infrared Calibration of Standard Stars by the Midcourse Space Experiment*, AFRL–VS–HA 2004–1109.